

Ultrafast Energy Transfer in Water–AOT Reverse Micelles

Dan Cringus,[†] Artem Bakulin,[†] Jörg Lindner,[‡] Peter Vöhringer,[‡]
Maxim S. Pshenichnikov,^{*,†} and Douwe A. Wiersma[†]

Department of Physical Chemistry, Zernike Institute for Advanced Materials, University of Groningen, Nijenborgh 4, 9747 AG Groningen, The Netherlands, and Institut für Physikalische und Theoretische Chemie, Rheinische Friedrich-Wilhelms-Universität, Wegelerstrasse 12, 53115 Bonn, Germany

Received: March 23, 2007; In Final Form: July 18, 2007

A spectroscopic investigation of the vibrational dynamics of water in a geometrically confined environment is presented. Reverse micelles of the ternary microemulsion H₂O/AOT/*n*-octane (AOT = bis-2-ethylhexyl sulfosuccinate or aerosol-OT) with diameters ranging from 1 to 10 nm are used as a model system for nanoscopic water droplets surrounded by a soft-matter boundary. Femtosecond nonlinear infrared spectroscopy in the OH-stretching region of H₂O fully confirms the core/shell model, in which the entrapped water molecules partition onto two molecular subensembles: a bulk-like water core and a hydration layer near the ionic surfactant headgroups. These two distinct water species display different relaxation kinetics, as they do not exchange vibrational energy. The observed spectrotemporal ultrafast response exhibits a local character, indicating that the spatial confinement influences approximately one molecular layer located near the water–amphiphile boundary. The core of the encapsulated water droplet is similar in its spectroscopic properties to the bulk phase of liquid water, i.e., it does not display any true confinement effects such as droplet-size-dependent vibrational lifetimes or rotational correlation times. Unlike in bulk water, no intermolecular transfer of OH-stretching quanta occurs among the interfacial water molecules or from the hydration shell to the bulk-like core, indicating that the hydrogen bond network near the H₂O/AOT interface is strongly disrupted.

1. Introduction

Spatial confinement phenomena are of fundamental importance for a vast number of research topics in physics, chemistry, and the life and medical sciences. For example, confinement of water in one or more spatial dimensions has important implications for many biological and biochemical research topics. Nanoscale water cavities and interfacial hydrophobic interactions are central ingredients in controlling the formation of the tertiary structure of proteins and hence ascertaining their proper functioning in living organisms. Transmembrane water wires either stabilized by globular peptides and proteins or spontaneously created as short-lived transient defects, play a critical role in the transport of charged or neutral particles across biological boundaries and, therefore, in the communication between cells and compartments within.

Recently, the ultrafast molecular dynamics (MD) of liquids that are geometrically confined on a nanometer scale have attracted considerable attention. Time-resolved femtosecond spectroscopy has been able to explore the ultrafast processes involved in aqueous solvation of optical probe molecules attached to proteins,^{1,2} nucleic acids,³ membranes,⁴ micelles,^{5–7} and artificial supramolecular nanoreceptors.⁸ These studies have uniquely demonstrated that the collection of motional degrees of freedom of water in the vicinity of the confining host matrix is strongly modified in comparison to that in the aqueous bulk phase.

In this spirit, many recent studies^{9–17} have focused on elucidating the inter- and intramolecular vibrational relaxation and spectral diffusion dynamics of water restricted to reverse

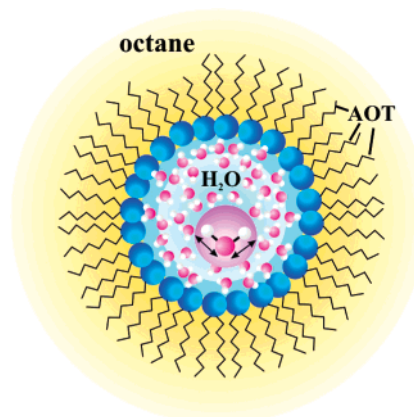


Figure 1. Schematic cross-section through a reverse micelle. The water droplet is surrounded by the AOT membrane, and the whole aggregate is immersed in a nonpolar solvent.

micellar environments. In these systems, nanometer-sized water droplets are immersed in a nonpolar hydrophobic liquid. The miscibility of the two otherwise immiscible liquids is facilitated by a coverage of the water nanodroplet with a monolayer composed of amphiphilic surfactant species such as bis-2-ethylhexyl sulfosuccinate (AOT; Figure 1). In these ternary mixtures, the distribution of micelle sizes is surprisingly narrow, with a polydispersity index around 10%.¹⁸ These systems can conveniently be described by their water-to-surfactant concentration ratio, w_0 , which is related to the average droplet radius by the relation $R_m(\text{nm}) = 0.15w_0 + 0.44$. The offset of 0.44 nm represents the empty volume of the micelle core in the absence of water when the surfactant headgroups are optimally packed to yield the highest interfacial curvature.¹⁹ AOT reverse

* Corresponding author. E-mail: M.S.Pshenichnikov@rug.nl.

[†] University of Groningen.

[‡] Rheinische Friedrich-Wilhelms-Universität.

micelles can be synthesized with w_0 ranging from 1 to more than 50, which corresponds to diameters from roughly one nanometer to a few tens of nanometers. It is also important that the structural integrity of the micellar supramolecular arrangement is warranted during time-resolved infrared pump–probe experiments.^{9–17,20}

Picosecond infrared spectroscopy on the OH-stretching mode of water droplets in microemulsions was performed for the first time by Graener and co-workers.^{10,11} The dynamics of thermal cooling of the reverse micelles on a time scale of several tens of picoseconds to nanoseconds were observed following the deposition of a certain amount of heat via pulsed infrared excitation of the OH-stretching vibration. The observed cooling dynamics were successfully simulated by a classical heat conduction model, in which the rate of the thermal relaxation was entirely determined by the droplet radius. However, the time resolution of this work was insufficient to reveal the primary vibrational relaxation, facilitating energy flow away from the initially excited OH stretching mode. Since then, two major directions have been pursued to obtain insight into the elementary energy transfer pathways and their associated time scales subsequent to an initial mid-infrared vibrational excitation.

In one approach, the focus was on the vibrational relaxation dynamics of the OH-stretching mode of neat H₂O droplets confined in reverse micelles.^{9,12} The corresponding spectral region is easily accessible and sensitive to changes in the hydrogen-bonded network originating from the spatial confinement of the water pool. The stretching OH vibration was excited by an ultrafast resonant mid-IR pump pulse, and the kinetics of the vibrational energy relaxation were followed with a variably delayed probe pulse in the same spectral region. Our previous results demonstrated⁹ that the full size-dependent spectrotemporal response in the OH-stretching region can be quantitatively predicted by a unified model that involves the weighted sum of two independently relaxing water subensembles: a bulk-like core located at the center of the droplet, and a surfactant-bound shell representing interfacial water (the “core/shell model” as named in a year-later publication¹⁶). This analysis was based on experimental data from nuclear magnetic resonance,²¹ linear infrared^{22–25} and photon-echo spectroscopy,⁴ and MD simulations.²⁶ The necessity of a similar separation has also been demonstrated in the IR pump–probe experiments on water clusters dissolved in acetonitrile,²⁷ where two distinctly different time scales were established for the vibrational dynamics of interfacial versus inside-the-cluster hydroxyl oscillators. The model included a size-dependent partitioning of the water molecules over the two subensembles, and does *not* require the vibrational relaxation rate of the core water to vary with the droplet size. Full agreement between experiment and simulation was achieved for droplet sizes between 1 and 10 nm without modifying the vibrational lifetimes.

In contrast, the size-dependent dynamics observed by Bakker and co-workers¹² in a parallel study on H₂O reverse micelles were interpreted as an anomalous decrease of the lifetime with decreasing micelle size. In other words, true nanoconfinement effects were assumed to modify the vibrational relaxation rate of *all* water molecules entrapped in the micellar pool, regardless of their spatial location (the so-called “homogeneous droplet” model). The authors proposed that the nanoconfinement affects the vibrational relaxation by the truncating and therefore weakening of the hydrogen-bond network to which the excited OH-oscillator is coupled. In this study, no attempt has been made to separate the vibrational dynamics of interfacial water molecules from those of the core water.

Within the second approach, the isotopomer HDO was highly diluted in a reverse micellar droplet of H₂O^{13–16} or D₂O.¹⁷ On the basis of pump–probe and stimulated vibrational echo experiments in combination with equivalent bulk-water and salt-solution data, Fayer and co-workers reported the dynamics in confined water to be, on average, substantially slower than those in the aqueous bulk phase.^{13,15} In the preliminary analysis, all water molecules were treated as originating from a single ensemble, as implied by the homogeneous droplet model. However, it was pointed out that deviations between experiment and simulations might originate from interface-bound water that was not explicitly taken into account.¹³ Later, the analysis of Fourier transform infrared (FTIR), pump–probe, anisotropy, and vibrational echo experiments was refined¹⁶ by adopting the very same core/shell model previously used by us.⁹ It was convincingly demonstrated that the size-dependent absorption spectra and population relaxation dynamics could be explained in the framework of the core/shell model, while the spectral diffusion and anisotropy experiments could not.¹⁶ This was explained as being due to a dynamical exchange between the core and the shell that mixes up their individual properties. Finally, Bakker and co-workers¹⁷ also distinguished core molecules from interfacial ones by their different vibrational lifetimes, thereby providing further support for the core/shell model.

The published results on the orientational anisotropy decay of HDO in reverse micelles (no data reported for H₂O as yet) measured by polarization-resolved mid-infrared pump–probe spectroscopy are not as conclusive as the population kinetics. For instance, biexponential anisotropy relaxation was reported and attributed to two independent processes: a local angular motion of the OD-oscillator, and a global structural relaxation of the entrapped hydrogen bond network.¹⁴ Analysis of the anisotropy with a wobbling-in-a-cone model indicated that the orientational dynamics decelerate as the droplet diameter is decreased, suggesting an increasing rigidity of the nanopool. Obviously, the core/shell model is not capable of accounting for this phenomenon. In contrast, other authors¹⁷ argued that the core and interfacial HDO molecules have markedly different orientational mobilities, ranging from a 2–4 ps decay for the core water to more than 15 ps for the interfacial water, thereby giving favor to the core–shell model.

Despite some remaining controversies concerning dynamical experiments (i.e., anisotropy and echo-peak shift¹⁶), the core/shell model seems to be preferential for describing vibrational experiments on diluted HDO molecules. However, direct extrapolation of this model onto the reverse micelles filled with neat water (either H₂O or D₂O) is by no means warranted without a thorough verification. The crucial difference between neat water and its highly diluted isotopomer counterpart is the density of resonant oscillators (i.e., excited hydroxyl groups). In the diluted HDO case, OD (or OH) oscillators are spectroscopically decoupled from each other and from the solvent water (H₂O or D₂O, respectively), making the latter to act merely as a heat bath. In contrast, in neat water, the excited hydroxyl group is resonantly coupled to other hydroxyls through intra- and intermolecular interactions. The latter is thought to promote vibrational energy transfer among water molecules at a 100 fs time scale, thus causing the ultrafast anisotropy decay^{28,29} and memory loss,²⁹ both experimentally observed in bulk water. On the basis of these studies, it appears quite reasonable to believe that the intermolecular energy transfer would also occur between H₂O molecules entrapped in reverse micelles. In this case, an initial excitation of the interfacial OH groups would delocalize very quickly into the core subensemble, and vice versa. In such

a way, any dynamics that are specific to the shell or core water would be smeared away within 100 fs, defeating the core/shell model. In fact, the homogeneous droplet model¹² was built on the assumption that the sub-100 fs intermolecular transfer of vibrational energy characteristic for bulk water washes out individualities of core/shell water molecules in reverse micelles. Some indications of such dynamical exchange were recently reported by Piletic et al. for HDO/H₂O reverse micelles,¹⁶ where the relevant dynamics occur at a time scale that is 1 order of magnitude slower than that in neat water.

From the above considerations, it is obvious that the vibrational excitation dynamics in H₂O reverse micelles might differ quite dramatically from the ones containing HDO–H₂O/D₂O mixture. The fact that spectroscopically neat water (H₂O or D₂O) differs so strongly from HDO–H₂O/D₂O mixtures provides a unique opportunity for obtaining invaluable *structural* information. For instance, if it could be shown that, for some reason, the resonance exchange between shell and core water is blocked, this would mean that the water-to-water communication line via the hydrogen bond network is broken. From this, one could deduce the reason of such a blockage that has its origin in the underlying molecular structure. Note that, in the case of diluted HDO molecules, such a point of view is not applicable because the oscillators are well separated in space and therefore cannot resonantly interact.

In this paper, we present a spectroscopic study of the vibrational relaxation of the OH-stretching mode of H₂O entrapped in reverse micelles in an effort to unravel the influence of spatial confinement on the dynamics of *neat* liquid water (H₂O). Micelles were prepared with $1 \leq w_0 \leq 35$ corresponding to diameters from 1 to 10 nm. Compared to our previous experiments,⁹ a considerably improved signal-to-noise ratio allowed us to distinguish two different relaxation pathways for core and shell water molecules. On the basis of all available data, a unified model of vibrational relaxation is proposed that accounts for all the experimentally observed linear and nonlinear mid-infrared responses. Furthermore, by introducing polarization selectivity, anisotropy dynamics were measured in the neat-H₂O filled reverse micelles for the first time. In contrast to intuitive expectations that ultrafast intermolecular dynamics quickly smear out differences between the core and shell water, we demonstrate that these two “species” do not resonantly exchange vibrational energy. This is a strong indication that a spatial confinement affects the water dynamics primarily near the membrane and that interactions of the interfacial layer with the rest of the water droplet are severely hindered.

The paper is organized as follows: After a description of the experimental setup and techniques (section 2), we discuss rotation-free time-resolved experiments with a sub-100 fs time resolution (section 3). In section 4, we outline the kinetic model, which is considerably more refined as compared to the one used in our previous work to model femtosecond-mid-IR pump–probe data on aqueous nanodroplets.⁹ Section 5 is devoted to a quantitative and global description of experimental observations in the framework of the core/shell model. After the origin of the pump–probe signal is clarified (section 5.1), the anisotropy measurements are analyzed in section 5.2. We conclude with a discussion of the relaxation channels and the energy transfer processes that occur within the water nanodroplet.

2. Experimental Methods

Reverse micelles were prepared by mixing appropriate amounts of water (Aldrich, HPLC grade), AOT from Aldrich, and octane (Janssen Chimica). All substances were used as

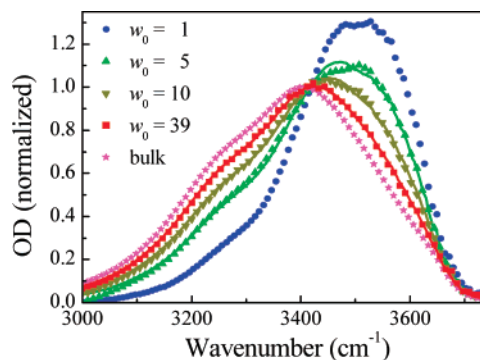


Figure 2. OH-stretching absorption band for four reverse micelle samples with different size and for bulk water (symbols). The solid lines are fits from the core/shell model. Spectra are normalized to the curve area.

received, without any further purification. To minimize contamination with water, the AOT was dissolved in octane immediately after the original container was opened. The residual water impurity of commercial AOT was estimated from the linear FTIR absorption spectrum to be on the order of 0.01 mL/g. This amount represents about 30% of the quantity added afterward for the preparation of the smallest micelles, and was taken into account when calculating the values of w_0 . For all the samples, the water concentration was about 0.3 mol/L, which corresponds to an optical density at the peak of the OH stretching band of about 0.4.

Figure 2 shows a comparison of the absorption spectra in the OH stretching region of water confined in reverse micelles with various diameters, and bulk water. The latter can be regarded as the limiting case of water entrapped in micellar droplets with an infinite diameter. To ease the comparison, the reverse micelle spectra were corrected for solvent contributions. In all cases, the stretching absorption band is rather broad and almost featureless, with spectral widths varying between 250 and 400 cm^{−1} full width at half-maximum (fwhm). The bulk water absorption is the broadest and most red-shifted spectrum. For rather large micelles ($w_0 = 35$), which contain tens of thousands of water molecules, the spectrum is slightly narrower and shifted to higher frequencies with respect to the bulk water spectrum. Decreasing the micelle size causes an even larger blue shift and a further narrowing. In general, such changes of the OH stretching absorption band reflect a restructuring of the hydrogen bond network.^{30,31} The blue shift and narrowing indicate that the water molecules on average are involved in fewer and/or weaker hydrogen bonds when they are confined to smaller droplets.^{32–34}

The blue shift and narrowing of absorption spectra with decreasing micelle size are quite similar to the observed trends in the HDO/H₂O filled reverse micelles.^{14–16} However, in contrast with the deuterium-substituted aqueous micelles, the width of the absorption spectrum of the H₂O-containing micelles changes monotonically with size.³⁵ The difference between the two cases is due to the much larger ratio of the spectral width over the blue shift (150/60 cm^{−1} for HDO/H₂O vs 350/70 cm^{−1} for H₂O), which underpins the dissimilarity between the neat water- (H₂O/H₂O) and HDO/H₂O-filled micelles.

Infrared femtosecond pulses were produced by an optical parametrical generator pumped by a 1 kHz Ti:sapphire multipass amplifier. The system has been described in detail elsewhere.³⁶ In short, the amplifier output (30 fs pulses centered at 790 nm) was split into four beams, the first of which was focused into a sapphire substrate to generate a white light continuum (WLC). The second beam was frequency doubled to 400 nm and

subsequently mixed in a β -barium-borate (BBO) crystal with a spectral band from the WLC centered around 640 nm. The resulting 1.1 μm idler wave was then parametrically amplified in two successive potassium titanyl phosphate (KTP) crystals, pumped by the remaining 800 nm beams. The output of this double-stage optical parametric amplifier (OPA) is filtered by a germanium plate to block the near-IR radiation (800 nm and 1.1 μm) and to transmit only its idler 3 μm branch. The mid-IR pulses were tunable around 3 μm and had a duration of about 70 fs with a bandwidth of 250 cm^{-1} fwhm.³⁶

The mid-IR output was collimated with a CaF_2 lens and was split by a CaF_2 substrate into an intense pump ($\sim 10 \mu\text{J}$ per pulse) and a weak probe ($< 1 \mu\text{J}$ per pulse) beams. The pump and probe pulses were temporally and spatially overlapped in the sample. Their relative time delay was adjusted by a computer-controlled optical delay line. The polarization of the probe beam was set at 45° with respect to the pump polarization, and an analyzer behind the sample selected either the parallel or the perpendicular component. To correct for systematic deviations between the scans with parallel and perpendicular polarizations, the corresponding data sets were tail-matched at long delays (> 10 ps) when the pump–probe signal became purely isotropic. The probe beam was subsequently dispersed by a 25 cm polychromator equipped with a 75 grooves/mm grating. The spectrum of the probe beam was recorded with a 64 elements mercury cadmium telluride (MCT) array, covering a spectral range of $\sim 500 \text{ cm}^{-1}$. Every other pump pulse was blocked by a 500 Hz synchronous chopper, and the pump–probe signal was calculated as the relative variation of optical density ΔOD in the presence and in the absence of the pump beam. For each spectrotemporal data set, 240 differential transient spectra consisting of 88 points were recorded for delays ranging from -3 to 10 ps with a step size between 20 and 100 fs for short and long delays, respectively.

For a single dipole transition, the pump-induced optical density $\Delta\text{OD}(\tau, \omega)$ (ω : probe frequency; τ : delay between pump and probe) of the sample is conventionally related to the population of the first excited-state and to the orientation of the excited dipoles. In this case, from the two pump–probe signals with orthogonal probe polarizations, one can obtain the isotropic (also known as rotational-free) component $\Delta\text{OD}_{\text{Rot-Free}}(\tau, \omega)$ and anisotropy $A(\tau, \omega)$ by using the following well-known expressions:³⁷

$$\Delta\text{OD}_{\text{Rot-Free}}(\tau, \omega) = \Delta\text{OD}_{\parallel}(\tau, \omega) + 2 \cdot \Delta\text{OD}_{\perp}(\tau, \omega) \quad (1)$$

$$A(\tau, \omega) = \frac{\Delta\text{OD}_{\parallel}(\tau, \omega) - \Delta\text{OD}_{\perp}(\tau, \omega)}{\Delta\text{OD}_{\parallel}(\tau, \omega) + 2 \cdot \Delta\text{OD}_{\perp}(\tau, \omega)} \quad (2)$$

From these relations, relaxation rates and rotational correlation times can be obtained, provided that care is taken to avoid well-documented pitfalls.³⁸

In general, any process triggered by the pump pulse that is accompanied by changes in the optical density of the sample in the probed spectral region yields an additional component to the pump–probe signal, which is dressed with its own orientational anisotropy. For instance, the excitation of an anharmonically coupled mode leads to changes in the central frequency and amplitude of the absorption cross-section of the probed mode without populating it. The coupled mode can be excited directly by a pump pulse with appropriate frequency, as is done in two-color experiments,^{39,40} but it can also be one of the modes that are populated transiently during the course of the relaxation processes. A typical example of the latter

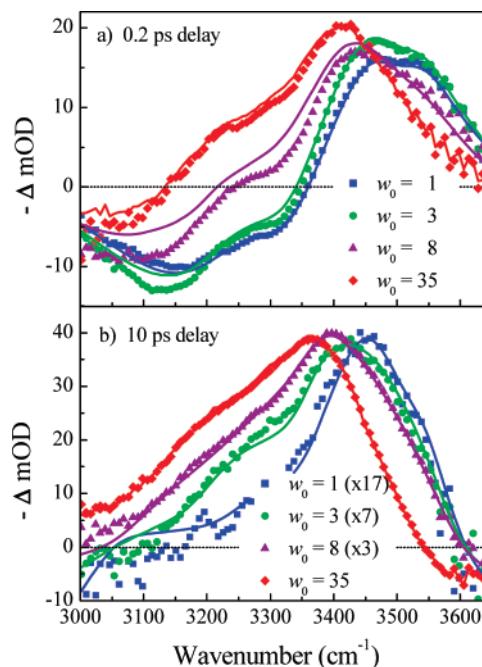


Figure 3. Transient spectra at a delay-time of 0.2 ps (a) and 10 ps (b) for w_0 equal to 1 (blue squares), 3 (green dots), 8 (purple triangles), and 35 (red rhombi). The solid lines show the simulations according to the core/shell model.

phenomenon is the excitation of low-frequency modes by heating of the sample volume.¹⁵ Moreover, the pump–probe signals might also be influenced by other dynamics, e.g., intra- or intermolecular energy transfer.^{28,29,41} When such additional processes are present, the population and reorientational kinetics described by eqs 1 and 2 do not have a straightforward interpretation, and require a more complex analysis. This issue will be discussed in detail in the following sections.

3. Population Relaxation

In this section, we present an overview of the rotation-free pump–probe signals. We begin by relating the spectral signatures observed in these measurements to the dynamical processes that occur in each sample, i.e., for each micelle size. Then, we identify the time scales associated with each of these phenomena. Finally, we summarize the relevant information needed to develop a model for the relaxation of the stretching-mode population.

Figure 3a shows the isotropic transient spectra for samples of different micelle sizes recorded at a pump–probe time delay of 0.2 ps. At such early times, the pump–probe signal is mostly dominated by the bleaching of the vibrational ground state as well as the emission from and absorption of the excited state of the OH stretching mode. Thus, for probing the $|0\rangle \rightarrow |1\rangle$ transition, i.e., between 3300 and 3600 cm^{-1} , the sample becomes more transparent, while, for probing the $|1\rangle \rightarrow |2\rangle$ transition, the optical density increases. The excited-state absorption is shifted to lower frequencies with respect to the $|0\rangle \rightarrow |1\rangle$ transition by the anharmonicity value of 200–250 cm^{-1} .^{9,40} Note that the frequency separation between maximum bleach and maximum absorption in Figure 3a is somewhat larger than this value because the spectral bandwidths of these components are comparable in magnitude to the anharmonicity shift.

The transient spectra at 10 ps delay (Figure 3b) deviate markedly from those recorded at 0.2 ps delay (Figure 3a), suggesting that the origin of the pump–probe signal completely

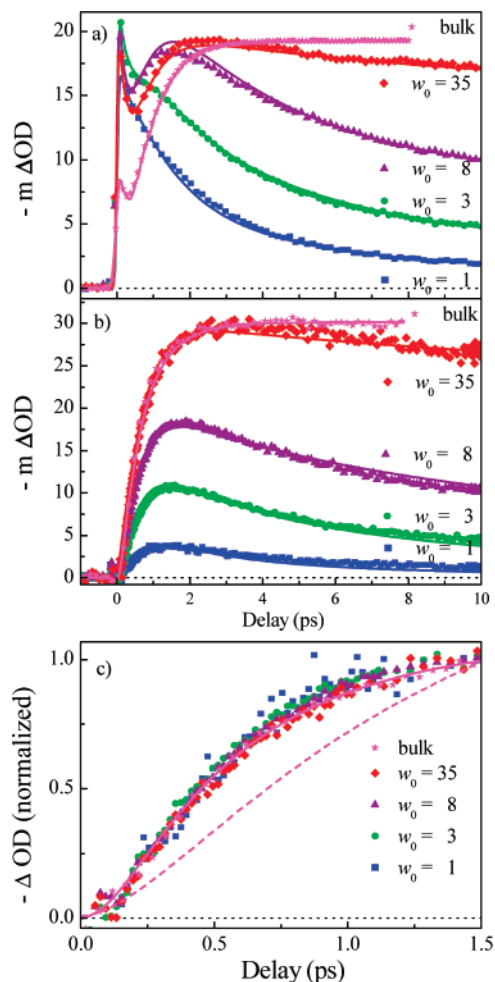


Figure 4. (a) Representative pump–probe transients for reverse micelles (at 3470 cm⁻¹) and bulk water (at 3410 cm⁻¹), together with fits from the core/shell model. (b) Pump–probe transients dominated by the thermalization signal. The solid curves in this panel show the normalized temperature evolution obtained from the simulations described in section 2 of the Supporting Information. (c) The data from panel b normalized at 1.5 ps, together with the bulk water model⁴⁰ calculations for the OH stretch relaxation time of 0.25 ps (magenta solid curve) and 0.85 ps (magenta dashed curve). In all panels, the symbols show the experimental points for reverse micelles with w_0 equal to 1 (blue squares), 3 (green dots), 8 (purple triangles), and 35 (red rhombi) and bulk water (magenta stars).

changes with time. The relaxation of the OH-stretching vibrational energy eventually leads to an increased water temperature in the focal volume. The OH stretching absorption band is very sensitive to variations in temperature⁴² because, at higher temperatures, water forms, on average, weaker and fewer hydrogen bonds,^{33,34,43} thereby shifting the vibrational resonance to higher frequencies. Thus, at long-time delays, the pump–probe signal reflects the absorption cross-section difference between the sample at an elevated temperature (i.e., pump pulse is present) and at room temperature (pump pulse is absent).^{9,10,40,44}

The time dependence of the two dynamical contributions to the pump–probe signal, namely, OH-stretching population relaxation on one hand and thermalization with heating of the observation volume on the other hand, is discussed more conveniently in terms of the time-resolved transients. Several representative isotropic pump–probe transients for micellar and aqueous bulk samples are shown in Figure 4a. These were recorded with detection frequencies located near the maximum of transient bleach/stimulated emission (i.e., 3470 cm⁻¹ for the

micelles and 3410 cm⁻¹ for bulk H₂O; see also Figure 3). In the case of bulk water (magenta asterisks), the amplitude of the bleaching signal recovers after a decrease following the initial rise and then remains constant during our experimental time window. At times under 2 ps, the signal for the largest micelles (red diamonds) follows the same trend as for bulk water. However, instead of leveling off at a constant bleach, it begins to decay on a time scale well in excess of several picoseconds. This long-time decay clearly depends on the micelles size and becomes faster with decreasing droplet diameter. For smaller micelles ($w_0 = 3$, green dots), this decay effectively competes with the delayed picosecond rise of the bleach resulting in a pronounced shoulder at a delay of ~ 1 ps. Finally, for the smallest micelles ($w_0 = 1$, blue squares), even the shoulder disappears, and the signal decays monotonously from a maximal initial bleach to a small offset imposed by the thermal contribution. However, this simple decay does not at all imply that the kinetics are less complex for the smallest micelles. Rather, the individual dynamical processes occurring after an initial vibrational excitation take place on comparable time scales and, therefore, cannot be visually distinguished from a single transient. For that, a more elaborated treatment based on a unified model is required (see section 4).

As discussed above, the decay following the initial rise of the transients shown in Figure 4a mainly reflects the stretching mode depopulation, while, for delays longer than 1 ps, the signal tracks the temporal evolution of the water temperature. Thus, for bulk water (magenta asterisks), the temperature increases and then remains constant, as the excess energy is equilibrated over the focal observation volume. The heat flux outside the focal volume occurs much slower and does not influence the data on the time scale of our experiments. The evolution of the water temperature in the reverse micelle samples is more complex because a heating of the droplet through thermalization of the excess vibrational energy is followed by a cooling of the droplet due to the heat flux away from the micelle and into the solvent.^{10,11}

Information about the thermalization dynamics in different samples is obtained rather quickly by inspecting pump–probe transients recorded at detection frequencies that are insensitive to the population dynamics, i.e., at probe frequencies for which the isotropic transient spectrum vanishes at short delay times (Figure 3a). The symbols in Figure 4b show such thermalization-only sensitive transient signals. In all cases, the temporal behavior of the pump–probe data is qualitatively identical, i.e., a bleaching signal rises within 2 ps as the temperature of the water droplet increases upon thermalization of the excess vibrational energy. Subsequently, the signal decays following the heat diffusion out of the water pool into the surrounding oil phase. The cooling rate depends on the micelle size, ranging between a few picoseconds for the smallest micelles (blue squares) and tens (red diamonds) or even hundreds of picoseconds for the largest droplets.^{10,11} At longer delays, the thermalization signal reaches saturation (not shown), as the whole focal volume is heated homogeneously.

The stretching mode depopulation, which is the first elementary step required for energy thermalization, appears to be slower in smaller micelles.^{9,12,13} Thus, one would expect a delayed temperature raise in smaller micelles compared to larger ones. This idea can be directly verified by normalizing the transients at a delay of 1.5 ps. At this delay, the signals are not significantly influenced by the ultimate cooling and therefore primarily reflect the process of heat production within the entrapped water pool. Quite surprisingly, normalized in such a way, thermalization

signals build up on an *identical* time scale regardless of the micelle diameter (see Figure 4c). Furthermore, they are even indistinguishable from the equivalent signal obtained for the bulk water sample. Finally, the temporal rise of temperature is also in perfect agreement with our previously published simulations⁹ of pump–probe experiments on aqueous bulk water samples using a lifetime of the OH-stretching mode of 0.24 ps (Figure 4c, solid curve). All together, these findings strongly suggest that, in all cases, the temperature jump originates from the relaxation of the same type of molecules, located in the bulk-like core of the micelle.

In contrast to the bulk core, interfacial water seems to transfer its vibrational energy directly away from the droplet into the micelle wall and the surrounding oil phase. Such an interpretation is in line with ref 20 and is based on the observation that the thermalization signal in small micelles ($w_0 = 1\text{--}2$) builds up faster than expected from the same bulk water simulation when using the accepted OH-stretching mode lifetime of 850 fs for small micelles^{9,12} (Figure 4c, dashed magenta curve). It is also interesting to note that the maximum transient temperature during vibrational relaxation/thermalization is lower in smaller micelles. This further supports the idea that only a fraction of the initially excited molecules contribute to heating of the water pool in small micelles. The remainder apparently follows a different relaxation mechanism.

To model the thermalization process, we solved numerically the classical heat diffusion equation for various micelle diameters (for details, see Supporting Information). Our simulations extend the previous studies by Graener and co-workers^{10,11} performed on relatively large micelles ($w_0 > 20$), to the smallest ones ($w_0 \sim 1$). The good agreement between experiment and simulations (Figure 4b, solid curves) demonstrates that reducing the properties of the micellar water pool to those of bulk water suffices in describing the essential features of the thermal processes, even for 1 nm-sized objects.

4. Kinetic Model

In this section, a relaxation model for the OH stretching mode of water in reverse micelles is constructed. A similar approach has been previously used to describe the vibrational relaxation and hydrogen bond dynamics in alcohol clusters.^{45,46} Here, we consider the specific pathways for vibrational relaxation that have been recently established in bulk water.^{40,47,48} We then adapt the model to describe the vibrational relaxation in aqueous nanodroplets of reverse micelles.

As was shown in ref 40, some details of the relaxation process can only be revealed through a global analysis of a complete set of multicolor experiments covering the stretching, bending, and librational spectral regions. Such comprehensive data sets are generally not accessible through a single “pump–stretch–probe–stretch” experiment. Therefore, when modeling a stretch–stretch experiment alone, the number of free parameters must be reduced substantially to avoid ambiguities of the fitting results. Since the present study focuses on the dynamics of the water OH-stretching mode, we will use a simplified model of vibrational relaxation in bulk water originally proposed by Lock and Bakker⁴⁷ that introduces several approximations in the relaxation scheme without affecting the major conclusions.

In bulk liquid water, several components, which reflect different steps in the relaxation of the OH stretching mode, contribute to the pump–probe signal.^{40,47,48} About 20% of the excess energy relaxes directly into librations, while 80% is transferred, presumably via the bend overtone serving as a very short-living doorway state, to the bending mode of two different

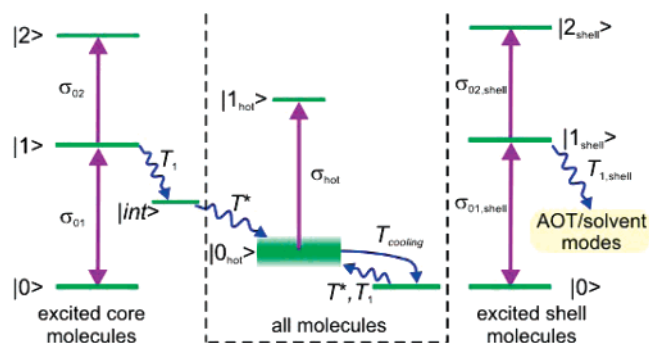


Figure 5. Energy level diagram for the kinetic model. The stretching mode of the core molecules relaxes, predominantly via an intermediate state, $|int\rangle$, to the “hot ground state”, $|0_{hot}\rangle$, which corresponds to an increase in the temperature of all water molecules. In the case of interfacial water, the stretch energy flows directly outside the water droplet. The “hot ground state” is depopulated following the heat diffusion into the solvent.

molecules. Subsequently, the bending energy is redistributed through the librational manifold, and, finally, the relaxation is terminated by the thermalization of the sample. Each of these steps affects the absorption cross-section in the stretching region, because of its coupling with the OH stretching mode. An interesting aspect revealed in ref 40 is that all these couplings are mediated by the hydrogen bond network in the following way: The excitation of various modes leads to a weakening of the hydrogen bond network, which in turn produces a blue shift of the stretching band.³² Therefore, the individual components of the pump–probe signal associated with the anharmonic couplings have similar differential cross-sections but different time evolutions.

On the basis of these considerations, we simplify the energy level diagram to the very minimum required to explain the major spectrotemporal features, namely, the relevant time scales and the difference between the pump–probe cross-sections at short and long delays. Thus, the pump–probe signal is separated into two components with different cross-sections: one component is related to the population of the stretching mode, and the other one accounts for the couplings between the stretching mode and all the other modes that become populated during the energy relaxation. The first contribution (bleaching at fundamental frequency and induced absorption at $|1\rangle \rightarrow |2\rangle$ transition frequency) decays according to the relaxation rate of the stretching mode. The second one builds up following the stretch relaxation and accounts for the anharmonic couplings of the stretching mode with the transiently populated bending, librational, and low-frequency modes. For bulk water, this component grows visibly slower than the stretching mode relaxes^{9,40,47} (Figure 4). This evolution is efficiently accounted for in the model by taking into account that the relaxation proceeds partially through a dark intermediate state, which effectively delays the sample thermalization.^{9,47}

Figure 5 summarizes schematically the ideas behind the kinetic model for the energy relaxation. Compared to the bulk water model by Lock and Bakker,⁴⁷ our modifications account for the heat diffusion from the water nanodroplets into the solvent^{9,11} in a similar way as done in the studies on alcohol clusters,^{45,46} and for the different vibrational relaxation channel for the interfacial water.²⁰ The energy deposited by the pump pulse into the first excited state of the stretching mode of bulk water molecules flows via an intermediate state to the “hot ground state”, $|0_{hot}\rangle$. For bulk water samples, the dynamics observable through a pump–probe experiment are basically terminated at this point because the average temperature in the

focal volume remains constant for times longer than the accessible observation window. The heat diffusion out of the focal volume occurs on microsecond time scales and can therefore be disregarded in the model. In contrast, the characteristic time for heat flux from the entrapped water into the surrounding octane depends on the micelle size, and ranges between a few picoseconds to several hundred picoseconds.

The populations of the relevant modes can be calculated from the following rate equations:

$$\frac{dN_1}{dt} + \frac{N_1}{T_1} = 0 \quad (3)$$

$$\frac{dN_{1,\text{shell}}}{dt} + \frac{N_{1,\text{shell}}}{T_{1,\text{shell}}} = 0 \quad (4)$$

$$\frac{dN_{\text{int}}}{dt} + \frac{N_{\text{int}}}{T_{\text{int}}} - (1 - a) \frac{N_1}{T_1} = 0 \quad (5)$$

$$\frac{dN_{\text{hot}}}{dt} - a \frac{N_1}{T_1} - (1 - a) \frac{N_{\text{int}}}{T_{\text{int}}} = 0 \quad (6)$$

In these equations, T_1 , N_1 and $T_{1,\text{shell}}$, $N_{1,\text{shell}}$ are the lifetimes and the populations of the OH-stretching mode of core and interfacial water molecules, respectively; T_{int} and N_{int} denote the lifetime and population of the intermediate state, and N_{hot} stands for the hot ground state population. In eqs 3–6, we accounted for the different relaxation pathways for core and shell water molecules (Figure 5). Since the H₂O molecules from the shell transfer their energy directly to the AOT molecules and the surrounding hydrophobic solvent²⁰ (see previous section), they neither contribute to the population of the intermediate nor the hot ground state of the core water. In analogy to aqueous bulk samples, the OH-stretching mode of the core water relaxes directly to the hot ground state with probability a , or via the intermediate state with probability $1 - a$. Equations 3–6 are solved analytically to result in the following temporal evolution of the populations:

$$N_1(\tau) = N_0 e^{-\tau/T_1} \quad (7)$$

$$N_{1,\text{shell}}(\tau) = N_{0,\text{shell}} e^{-\tau/T_{1,\text{shell}}} \quad (8)$$

$$N_{\text{int}}(\tau) = N_0(1 - a) \frac{e^{-\tau/T_{\text{int}}} - e^{-\tau/T_1}}{T_{\text{int}} - T_1} T_{\text{int}} \quad (9)$$

$$N_{\text{hot}}(\tau) = N_0 \left[a(1 - e^{-\tau/T_1}) + (1 - a) \left(1 - \frac{T_{\text{int}} e^{-\tau/T_{\text{int}}} - T_1 e^{-\tau/T_1}}{T_{\text{int}} - T_1} \right) \right] \quad (10)$$

where N_0 and $N_{0,\text{shell}}$ are the respective populations of the initially excited water molecules.

The depopulation of the hot ground state due to heat flux from the micelles into the solvent can be accounted for in a phenomenological fashion by introducing an additional relaxation term with the characteristic cooling time T_{cooling} . A more rigorous approach should involve a numerical solution of the heat diffusion equation as presented in the Supporting Information. However, because the dynamics of cooling are temporally separated from those of vibrational relaxation, an exponential

cooling term provides a reasonable approximation that greatly reduces computation time.

With these considerations, the changes in the optical density of the sample volume experienced by the probe beam are described by the following expression:

$$\Delta\text{OD}(\omega, \tau) \propto f_{\text{core}} [\sigma_{12}(\omega) - 2\sigma_{01}(\omega)] N_1(\tau) + f_{\text{shell}} [\sigma_{12,\text{shell}}(\omega) - 2\sigma_{01,\text{shell}}(\omega)] N_{1,\text{shell}}(\tau) + f_{\text{core}} [\sigma_{\text{hot}}(\omega) - \sigma_{01}(\omega)] [(\beta - 1)e^{-\tau/T_{\text{cooling}}} + 1] N_{\text{hot}}(\tau) \quad (11)$$

where $\sigma_{01}(\omega)$, $\sigma_{12}(\omega)$ and $\sigma_{01,\text{shell}}(\omega)$, $\sigma_{12,\text{shell}}(\omega)$ are absorption cross-sections corresponding of the $|0\rangle \rightarrow |1\rangle$ and $|1\rangle \rightarrow |2\rangle$ transitions of the core and shell water, respectively. The quantities f_{core} and f_{shell} are the fractions of the molecules of the core and shell subensembles, and they fulfill the condition $f_{\text{core}} + f_{\text{shell}} = 1$. The absorption cross-section of the $|0_{\text{hot}}\rangle \rightarrow |1_{\text{hot}}\rangle$ transition is denoted as $\sigma_{\text{hot}}(\omega)$. The parameter β is a measure of the heat redistribution and represents the ratio between the maximum theoretical water temperature in the absence of heat flux through the membrane and the actual water temperature in the presence of heat flux after full thermalization of the entire focal observation volume. If $\beta = 1$, as is the case for bulk water, no heat flux occurs. In the opposite case, if $\beta \rightarrow \infty$, the fraction of the focal volume occupied by the solvent is much greater than the portion occupied by the micelles.

Finally, we point out that the model presented above is not aimed at describing the complete relaxation process from the stretching mode to the ground state in all details. Rather, it is meant to provide reliable information on the dynamics of the stretching mode by approximating the contributions arising from anharmonic couplings to the bending and librational modes with a minimum of adjustable parameters.^{9,47} The kinetic scheme presented here generalizes our previously proposed model⁹ by taking into account the difference in relaxation channels for the core and shell water molecules.

5. Analysis and Discussion

In this section, the isotropic and anisotropic pump–probe transients are analyzed in detail in terms of the kinetic core/shell model outlined above. In particular, the energy transfer pathways and relaxation rates are established. This information is used to interpret the anisotropy data, which are shown to be significantly affected by the thermalization processes.

5.1. Rotation-Free Pump–Probe Signals. We start our data analysis by fitting the generalized kinetic model introduced in the previous section to the experimental data sets for four micelle sizes: $w_0 = 1$, $w_0 = 3$, $w_0 = 8$, and $w_0 = 35$. An overview of all parameters is given in Table 1. The parameters defining the vibrational relaxation (T_1 , T_{int} , and a) are identical in all four cases and in agreement with previous studies on bulk water.^{9,40,47} Because the cooling of the entrapped water droplet is sensitive to the micelle size, the time constant T_{cooling} was used as a free fitting parameter. The differential cross-section for the thermalization signal of each micelle's size was obtained from the pumped-induced differential transmission spectrum recorded at relatively long time delays (> 10 ps) when vibrational relaxation is complete. The simulation was initially carried out for the data from the largest micelles because their relaxation times are expected to match those already determined previously for bulk water.^{9,40,47} Equipped with the parameters values that define the heating process (T_1 , T_{int} , and a) found from the simulation of the $w_0 = 35$ sample, the vibrational relaxation time of the shell water in the smallest micelles ($w_0 = 1$) was derived next. Finally, for intermediate sizes, the difference absorption cross-sections

TABLE 1: Parameters of the Kinetic Model Derived from the Data Fits

model parameter		micelle size				bulk water
notation	meaning	$w_0 = 1$	$w_0 = 3$	$w_0 = 8$	$w_0 = 35$	
T_1	excited-state lifetime of core water			0.27 ps		0.25 ps
$T_{1,\text{shell}}$	excited-state lifetime of shell water			0.85 ps		N/A
T_{int}	intermediate state lifetime			0.55 ps		0.55 ps
a	branching ratio			0.25		0.25
T_{cooling}	effective cooling time	3.5 ps	5.2 ps	6 ps	12 ps	∞
β	heat redistribution parameter	6.7	5.4	3.5	1.3	1.0
f_{core}	fraction of core molecules	0.05	0.22	0.52	0.9	N/A
f_{shell}	fraction of shell molecules	0.95	0.78	0.48	0.1	N/A

for the core ($\sigma_{01}(\omega) - 2\sigma_{12}(\omega)$) and interfacial ($\sigma_{01,\text{shell}}(\omega) - 2\sigma_{12,\text{shell}}(\omega)$) water are fixed to those obtained for $w_0 = 1$ and $w_0 = 35$, respectively, with their amplitudes being fit parameters.

Figure 6 displays the frequency-resolved pump–probe data for the four micelle sizes in a false-color representation. The experimentally obtained data (upper panels) can be directly compared with the results of the least-squares fitting procedure described above (lower panels). For the largest micelles (Figure 6, right column), the best fit with $f_{\text{shell}} = 0$ is achieved with a core stretching mode lifetime $T_1 = 0.27 \pm 0.05$ ps, an intermediate mode lifetime $T_{\text{int}} = 0.55 \pm 0.05$ ps, a cooling time $T_{\text{cooling}} = 12 \pm 2$ ps, and a branching ratio $a = 0.25$. The first two parameters are close to those found for bulk water, showing that, in the largest micelles ($w_0 = 35$), the population kinetics mimic that of bulk water.^{9,40,47} Still, the stretching mode lifetime is slightly longer than in the bulk. This deviation is likely due to the small but finite amount of interfacial water.

In the smallest micelles ($w_0 = 1$), most of the entrapped water is interfacial, i.e., $f_{\text{core}} \ll f_{\text{shell}}$. Thus, the biexponential decay corresponding to the stretching mode depopulation (first two terms in eq 11) is dominated by the relaxation of the interfacial molecules, while the population relaxation term for bulk-like molecules is negligibly small. Furthermore, the two parameters $T_{\text{int}} = 0.55$ ps and $a = 0.25$ are already known and therefore fixed before fitting eq 11 to the experimental data. The quality of the fit can be assessed by comparing the panels in the left column of Figure 6. The fitting procedure yields an average cooling time of 3.5 ± 0.3 ps and an OH-stretching lifetime for the interfacial water molecules $T_{1,\text{shell}} = 0.85 \pm 0.1$ ps. This lifetime is more than three times longer than that in bulk

water,^{9,40,47} where the stretch relaxes mainly into the bending mode, most probably with the bending overtone acting as a doorway state.^{40,47}

For a broad range of hydrogen-bonded systems, it has been shown that the OH-stretching lifetime correlates with the spectral position of the corresponding linear absorption band.⁴⁹ According to this relation, the stretch lifetime for interfacial water should be ~ 0.4 ps,¹² which is roughly a factor of 2 shorter than the experimental value determined for AOT-bound water of the smallest micelles. This observation suggests that the OH-stretching relaxation pathways for interfacial water and for bulk water are fundamentally different. Dlott and co-workers proposed that the AOT molecules covering the water nanodroplet directly channel the initial OH-stretching excess energy of the H₂O-molecules bound to the AOT headgroup into the surrounding oil phase.²⁰ This mechanism is also in line with a rise-time of the heating process that is independent of the droplet size (section 3), and with our observation of the amplitude of the thermal component in smaller micelles, which is lower than expected from the number of excited water molecules within the reverse micelle. All these findings indeed indicate that most of the interfacial water molecules transfer their stretching energy directly to the membrane and then into the surrounding octane solvent, while only the residual bulk-like water molecules are able to convert their excess vibrational energy into heat deposited within the water nanodroplet.

For the intermediate-sized micelles, where the fractions of bulk-like core and interfacial water become comparable, the core/shell model imposes strict constraints. Their rotation-free signals must be modeled, while most of the fitting parameters

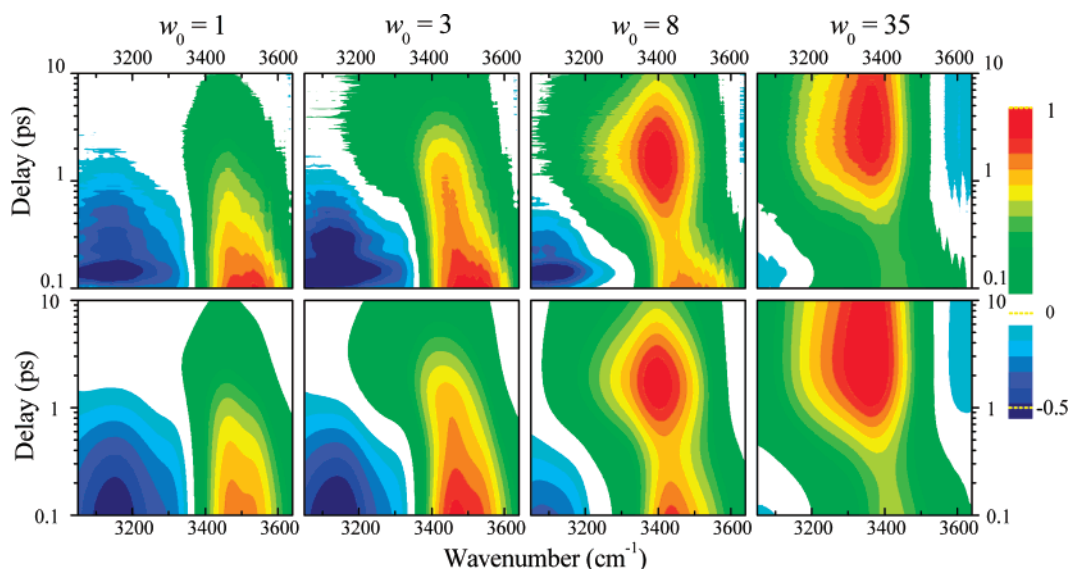


Figure 6. Normalized experimental rotation-free signals (top row) and best fits (bottom row) obtained on the basis of the core/shell model. Eighteen equally spaced levels separate the -0.5 and 1 values. The dark blue color indicates values lower than -0.5 , and white corresponds to absolute values smaller than 8.5% of the maximum.

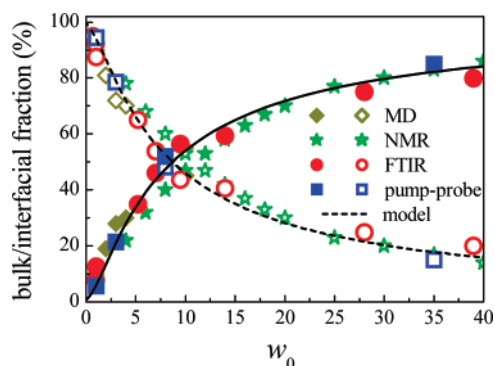


Figure 7. Decomposition into interfacial (open symbols) and bulk (solid symbols) fractions from MD simulations⁵⁰ (dark yellow diamonds), NMR⁵¹ (green stars), rotation-free pump–probe transients (blue squares), and linear spectra (red circles). Black curves: best fit to the geometrical model (for details, see section 1 of the Supporting Information).

are predetermined by the values obtained from the two limiting samples, namely, $w_0 = 1$ (for interfacial water) and $w_0 = 35$ (for core water). These parameters include the OH-stretch lifetimes for the two subensembles, the difference absorption cross-sections of the two limiting micelle sizes $w_0 = 1$ and 35, the intermediate mode lifetime, and the probability of direct relaxation to the ground state (Table 1). We recall that the thermalization cross-sections are fixed from separate measurements at long delays. In addition, the cooling times derived from the fits can be directly compared with those obtained from the data and the corresponding simulations solving the heat diffusion equation (see Supporting Information) shown in Figure 4b. Therefore, the *only* true fitting parameter that remains for simulating the data of intermediate-sized micelles is the ratio between core and interfacial water, $f_{\text{core}}/f_{\text{shell}}$. The middle panels in Figure 6 compare the observations with the fit results obtained in this fashion for droplets with intermediate diameters. Despite the rigid constraints on all time constants, the model is able to reproduce the experimental data very well.

For a consistency check of the core/shell model, we followed the same route as that proposed by Dokter et al. for HDO/D₂O reverse micelles and analyzed the size-dependent molecular fractions of the two entrapped water species.¹⁷ For the smallest and the largest micelles (i.e., $w_0 = 1$ and $w_0 = 35$), refined molecular fractions were determined by fitting once again the corresponding data with the same model while dropping the previously imposed constraints $f_{\text{core}} \ll f_{\text{shell}}$ and $f_{\text{shell}} = 0$, respectively. The relative fractions obtained in this way are displayed in Figure 7 as blue squares. The results are in excellent agreement with those obtained from MD simulations for small micelles⁵⁰ (Figure 7, dark yellow diamonds) and NMR studies for larger droplets⁵¹ (Figure 7, green asterisks). Furthermore, partitioning of the FTIR absorption spectra of reverse micelles onto core and shell components (for details, see Supporting Information), performed in a similar manner as in ref 16, is also in good agreement with the other data (Figure 7, circles). In addition, the fit of the geometrical model⁵¹ (Figure 7, black curves) yields a value of 0.36 nm for the thickness of the interfacial layer, which is close to the oxygen–oxygen distance in liquid water (0.29 nm) and in perfect agreement with the value obtained by Piletic et al.¹⁶ It is interesting to note that all characteristic values derived here for H₂O-filled micelles closely match those obtained for HDO/H₂O (ref 16) and HDO/D₂O (ref 17) filled micelles, thereby proving the independence of the fractional decomposition of the specific reverse micelle content. More important, this also suggests that the core and shell water

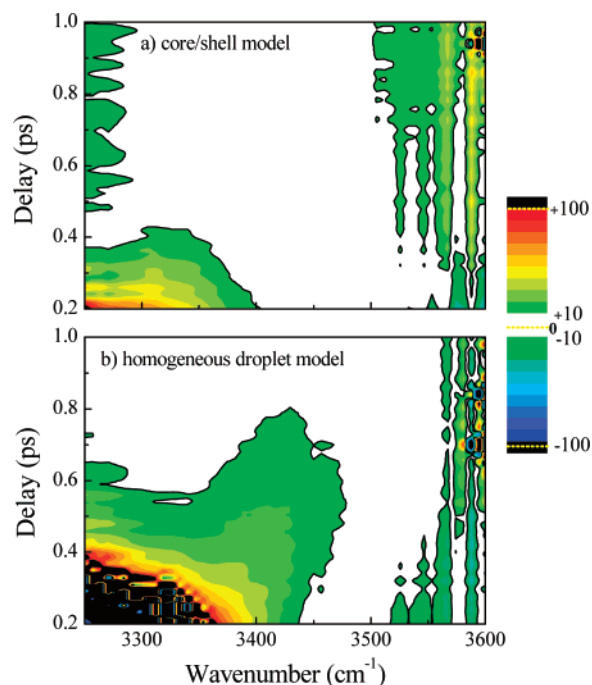


Figure 8. Relative deviation from experiment in the case of $w_0 = 8$ micelles for the core/shell model (a) and homogeneous droplet (b). The white region corresponds to deviations smaller than 10%. Twenty equally spaced levels separate the -100% (blue) and 100% (red) deviations. The black region shows values outside this range.

molecules do not exchange vibrational excitation, as otherwise the partition into the core–shell components would be distorted.

In order to further verify the validity of the core/shell model, we compared the quality of the fits obtained from it with simulations results within the homogeneous droplet model framework. The latter assumes a single relaxation channel (and therefore a single relaxation time) for all molecules, regardless of their spatial location within the micelle. Note that, counter-intuitively, the homogeneous droplet model requires a larger number of free fitting parameters because no constraints are imposed on the OH-stretching lifetime and the differential absorption cross-sections prior to simulating the data on an intermediate-sized micelle. Therefore, in this case, the time constant of the exponential decay describing the stretch relaxation is a free fitting parameter, and so are the corresponding amplitudes at each frequency. The parameters obtained in such fashion match the previously reported values.¹² The color-shaded contour plots in Figure 8 show the relative residuals between the experimental data and the simulation results based on the core/shell (a) or the homogeneous droplet (b) model for a micelle size of $w_0 = 8$. The white area corresponds to deviations smaller than $\pm 10\%$, and black areas correspond to deviations larger than $\pm 100\%$. Despite the lower number of free parameters, the core/shell model reproduces the experimental data much better than the homogeneous droplet model. The large relative residuals around 3250 cm^{-1} originate from an (within signal-to-noise) almost vanishing pump–probe signal. Therefore, it is more informative to analyze the deviations around 3400 cm^{-1} , i.e., at the maximum pump–probe signal.

Even from time-independent measurements, such as FTIR and NMR spectra, it is clear that interfacial and bulk-like water in reverse micelles exhibit significant differences. These structural heterogeneities are described straightforwardly in the framework of the core/shell model. It is natural to presume that the same structural separation is valid for the dynamical processes occurring within the droplet, and the same model

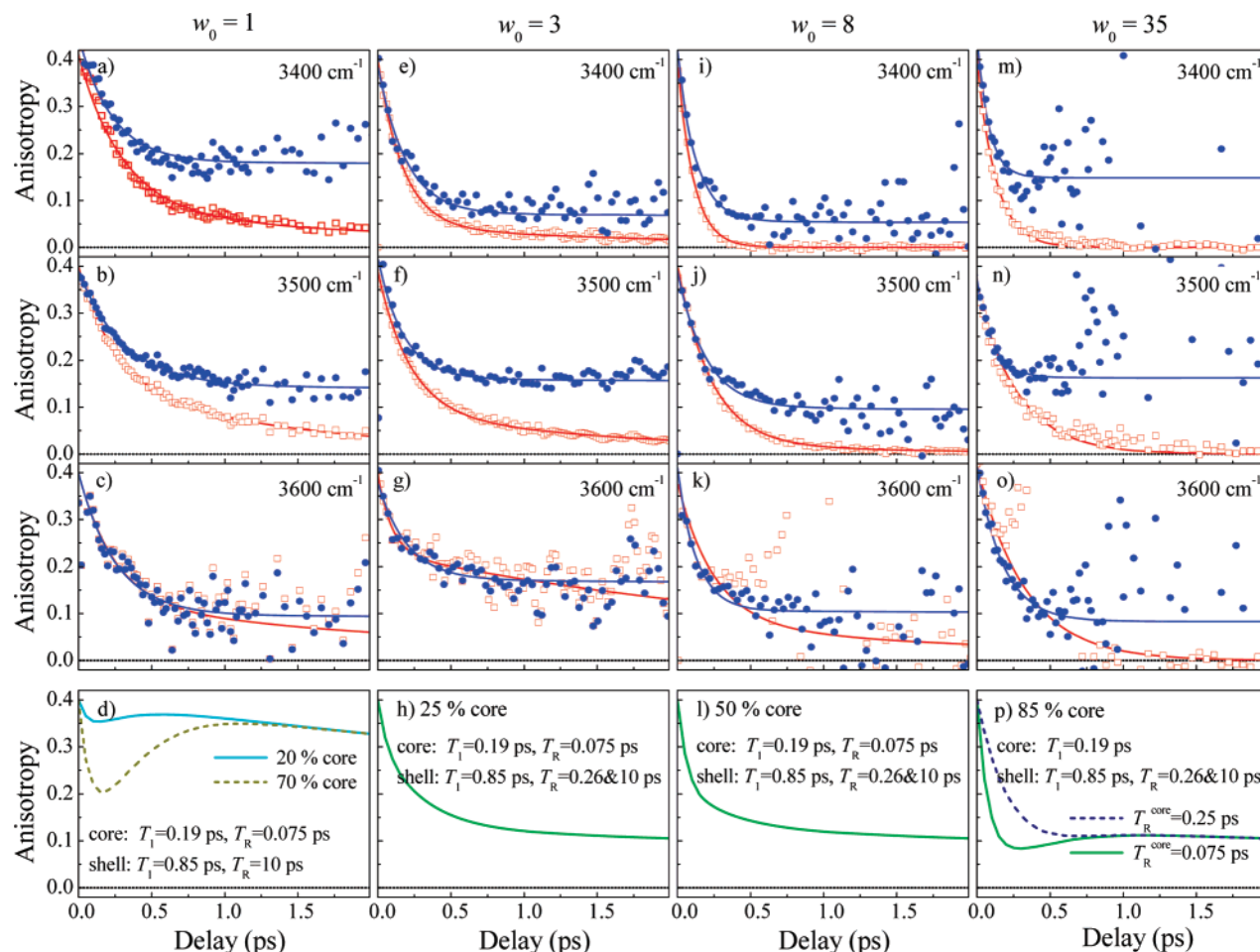


Figure 9. Typical anisotropy decays. The red squares show uncorrected anisotropy decays, and the blue dots show decays after subtraction of the thermalization component. Solid lines in the upper three panels for each micelle size are fits. Bottom panels: simulations for two components (see text for details).

should be used to describe the kinetics, as demonstrated in Figure 8. The main argument used previously to advocate the appropriateness of the homogeneous droplet model¹² is the measured increase of the OH— stretching mode lifetime from 0.26 to 0.39 ps in going from the aqueous bulk phase to water confined to reverse micelles with $w_0 = 12$. Bakker and co-workers argued that such an increase cannot be due to the presence of interfacial water with a lifetime of 0.85 ps because its abundance in the micelle was taken as a mere 10%. However, inspection of Figure 7 immediately demonstrates that this quantity was strongly underestimated, as the true content of the core water is $\sim 40\%$. Moreover, the same authors later¹⁷ critically reviewed the molar fraction of shell water and obtained values that are much closer to those displayed in Figure 7. With a realistic molar fraction for interfacial water that corroborates the majority of experimental data available in the literature, the *ensemble-averaged* OH-stretching lifetime is entirely consistent with the core/shell model.

From the above analysis, we can conclude that the pump—probe experiments on the water nanopools can be explained satisfactorily by the core/shell model. The thickness of the shell suggests that a spatial limitation of the hydrogen bond network affects the spectroscopic properties of the sample only over a distance of approximately one molecular layer. At larger distances from the membrane, the confined water shows spectral features that are identical to bulk water, without any variations expected from the homogeneous droplet model. As pointed out in the Introduction, the homogeneous droplet model¹² was built

on the assumption that the sub-100 fs intermolecular transfer of vibrational energy reported for bulk water^{28,29} is also present in reverse micelles. Therefore, the initial excitation of the interfacial OH groups would delocalize very quickly into the core water subensemble. As a consequence, any energy transfer dynamics specific to the interface-bound water would be inhibited. In contrast, the simulations of our experimental data strongly support the existence of different relaxation channels for shell and core water, implying that the two species do *not* efficiently exchange vibrational energy on a time scale shorter than the stretch lifetime. In the next section, we will show, on the basis of reorientational anisotropy measurements, that intermolecular energy transfer between shell and core water is *either very slow* (> 10 ps) *or does not occur at all*.

5.2. Anisotropy. For a molecular system consisting of a single spectroscopic transition dipole, μ , the anisotropy decay is a measure of the orientational correlation function, $\langle P_2[\mu(0)\mu(t)] \rangle$, where P_2 is the second-order Legendre polynomial, and the angular brackets denote an ensemble average.³⁷ In an ideal case, the anisotropy decay reveals the orientational randomization of the transition dipoles initially selected through excitation with a linearly polarized light pulse.^{52,53}

The time dependent anisotropy $A(\tau, \omega)$ calculated from the parallel and perpendicular transients according to eq 2 is displayed in Figure 9 for several micelle sizes at three representative probing frequencies (red squares). In all cases, the anisotropy at zero time delay is close to 0.4, which shows that all the relevant transient processes are captured. For smaller

micelles ($w_0 = 1$ and 3), the anisotropy decays biexponentially. The anisotropy drops to $\sim 50\%$ of the initial value with a time constant of 0.25 ± 0.05 ps. The short-time decay is followed by a slower tail decaying with a characteristic time constant of 2.5 ± 1 ps. For large micelles ($w_0 = 35$, right column in Figure 9), the anisotropy decay is noticeably faster, although it is slightly slower than the ~ 100 fs reported for bulk water.^{28,29} Fitting a single-exponential function to the data at various frequencies yields a decay constant of 0.25 ± 0.1 ps, without any evidence for a picosecond scale component.

The pure rotational diffusion of water has been investigated extensively by a wide variety of experimental techniques (for a compilation of data see, e.g., ref 54) and is likely to involve large amplitude angular jumps occurring concertedly with the cleavage and reformation of hydrogen bonds to nearest neighbors.⁵⁵ The time scale for full orientational scrambling is well in excess of one picosecond.^{14,27,56,57} In addition, from the rather small principal moments of inertia of water, the inertial decay of the orientational correlation function could be expected to be below 100 fs,⁵⁵ but its relative amplitude should be much smaller than the observed 50%. Therefore, it is unlikely that the fast initial decay evident in all micelle sizes is directly caused by reorientational dynamics.

The interpretation of the anisotropy data is complicated by the fact that the rotational diffusion is not the only process that can cause the loss of the preferential orientation of the excited dipoles. This is especially true for liquid water where the measurements are influenced by intermolecular^{28,29} and intramolecular⁴¹ transfer of vibrational energy, and thermal heating effects,⁵⁸ already discussed in section 4. Each of these processes affects the pump–probe transients obtained with parallel or perpendicular polarizations of the two beams. Because anisotropy $A(t)$ is calculated directly from these transients (see eq 2), the very same dynamics also influence the temporal behavior of the orientational anisotropy. In other words, the anisotropy decay is affected even if the processes that influence the parallel and perpendicular signals do not contribute directly to an angular randomization of the transition dipoles.⁵⁹

For instance, Förster-type hopping of vibrational excitations due to dipole–dipole interactions causes the anisotropy to decay without requiring a reorientational motion of the energy-donating or energy-accepting molecules.^{28,29} The intramolecular flow of vibrational energy between anharmonically coupled modes with transition dipoles having different orientations in the molecular frame also results in a loss of orientational memory. In water, this is the case when vibrational energy is transferred between the symmetric and asymmetric OH-stretching modes.^{41,60} If the relaxation pathway involves transitions that are anharmonically coupled to the mode being monitored by the probe beam, a nonlinear response is introduced, whose polarization dependence is connected to the symmetry of molecule.^{40,61} However, if the relaxation partitions the initial excess energy over several molecules that are probed, as is the case for the thermalization dynamics, an additional isotropic response emerges, which does not contain any information regarding the original angular distribution selected by the pump pulse.

Because of all these complexities, it is always mandatory to elucidate the origin of the pump–probe signal prior to analyzing and interpreting the anisotropy decay in terms of reorientational dynamics.¹⁶ Note that, in addition to the aforementioned processes, an accurate retrieval of the anisotropy from orthogonally polarized pump–probe data requires a sufficiently long lifetime. If the pump–probe transients decay to zero before angular randomization, the anisotropy decay will be over-

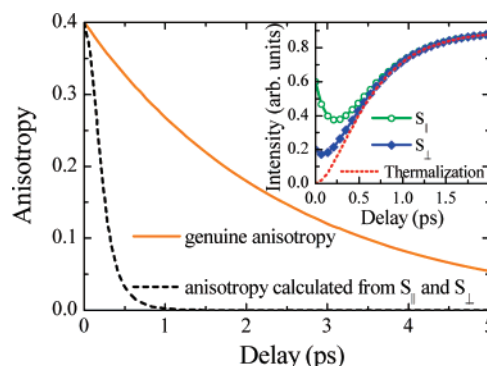


Figure 10. Inset: Modeling of parallel (green open circles) and perpendicular (blue solid rhombi) pump–probe signals and the corresponding thermalization signal (red dotted line). The main panel shows the anisotropy decay calculated from the signals in the inset (black dashed curve) and the genuine anisotropy decay of the system (orange solid curve).

whelmed by noise and does not have the dynamic range necessary for a reliable determination of the rotational correlation time.

In order to demonstrate the effect of thermalization dynamics on the transient anisotropy, let us consider a model system with a population relaxation time of 0.25 ps and a rotational diffusion time of 2.5 ps (Figure 10, orange solid curve), i.e., with typical time constants of bulk water.^{27,40,47,56} Following ref 16, we calculate the corresponding parallel and perpendicular pump–probe signals due to depopulation of the excited state. To these signals, a purely isotropic contribution (red dotted curve in the inset of Figure 10) is added that reflects the temperature rise due to redistribution of the deposited energy over low-frequency modes. The amplitude of this component was set to match typical pump–probe experiments on bulk H₂O.^{28,29,40} The transients obtained in this fashion (green empty circles and blue solid diamonds in Figure 10, inset) mimic experimental pump–probe signals on bulk H₂O, assuming that orientational scrambling is dictated only by rotational diffusion with an exponential time constant of 2.5 ps. The anisotropy constructed from these two signals is shown in Figure 10 as a black dashed curve. Fitting a single-exponential decay to this curve yields a time constant of ~ 0.2 ps, which is more than an order of magnitude shorter than the genuine anisotropy decay constant of 2.5 ps (orange solid curve). This example clearly illustrates that the apparent anisotropy decay time can be totally meaningless when the isotropic thermalization signal is not properly accounted for. In fact, the apparent fast anisotropy decay has little to do with the reorientational motion but rather reflects the population relaxation of the excited dipoles. This is because the denominator in eq 2 increases due to the growth of the isotropic thermal component, thereby causing an artificial acceleration of the anisotropy decay.

The above case study clearly shows that the thermal isotropic component to the pump–probe signal severely distorts the anisotropy decay. Therefore, it needs to be subtracted from the parallel and perpendicular transient signals before substituting them into eq 3.^{16,27,58} The following expression was derived in ref 16 in order to retrieve the correct depolarization rate:

$$R(\tau, \omega) = \frac{\Delta OD_{||}(\tau, \omega) - \Delta OD_{\perp}(\tau, \omega)}{\Delta OD_{||}(\tau, \omega) + 2 \cdot \Delta OD_{\perp}(\tau, \omega) - 3 \cdot \Delta OD_{\text{thermal}}(\tau, \omega)} \quad (12)$$

where $\Delta OD_{\text{thermal}}(\tau, \omega)$ denotes the thermal contribution. The

temporal evolution of this component can be independently observed at the frequency where the population contribution vanishes (Figure 4b) and then refined using the global fitting procedure described Section 4.

The first column of Figure 9 illustrates the effect of thermalization on the retrieved anisotropy in the case of small micelles ($w_0 = 1$). The blue dots show the anisotropy $R(t, \omega)$ calculated according to eq 12, i.e., with the thermal contribution properly subtracted. The initial 0.25 ps decay is not significantly affected when the thermalization signal is accounted for (compare red and blue symbols), while the slow component certainly is. As was demonstrated in context with Figure 10, the anisotropy appears to decay faster than the orientational correlation function when the thermal signal (red dots in the inset of Figure 10) is not subtracted. Thus, the 2 ps decay time found in this case should be considered as a lower limit for the rotational correlation time. After subtraction of the thermalization signal, this component decays on time scales on the order of a few tens of picoseconds. Unfortunately, this time constant is much longer than the vibrational lifetime (0.85 ps), and therefore an upper limit for the rotational correlation time cannot be specified.

From Figure 9, we can conclude that, for the smallest micelles, the anisotropy exhibits two distinct components. The first one causes the signal to decay to a value of 0.1–0.2 with a time constant of 0.25 ± 0.05 ps, while the second component is characterized by a time constant longer than 10 ps. This biphasic decay may have several physical origins, which we examine in detail below.

One possibility is that, even in the smallest micelles, there may still be a residual amount of bulk-like water (see Figure 7 and the references within), which is responsible for the fast initial decay, while the slow component (decay time > 10 ps) is due to the predominant interfacial water. In order to verify this hypothesis, we calculated the anisotropy that is expected from a system containing two types of water molecules with different vibrational relaxation and depolarization rates. In these simulations, we used $T_{1,\text{shell}} = 0.85$ ps and $T_{R,\text{shell}} = 10$ ps for interfacial water. Since $T_{R,\text{shell}}$ is large when compared to $T_{R,\text{core}}$, it does not influence the fast initial decay of $R(\tau, \omega)$, and the particular value of this time does not affect the following discussion. The bulk water subensemble in the micelle was assigned the values published in the literature for bulk water, namely, $T_1 = 0.19$ ps and $T_R = 0.075$ ps.²⁹ The cyan solid curve in Figure 9d depicts the anisotropy calculated for a mixture of 20% core water and 80% interfacial (shell) water. Clearly, the simulation does not even qualitatively resemble the experimental anisotropy, as, first, the amplitude of the fast initial decay is too small, and, second, the anisotropy displays an intermediate rising component, which is not observed in the experiment. Even if the bulk water concentration is increased to 70%, which is strongly exaggerated, the agreement between experiment and simulation (dark yellow dashed line) does not improve at all. Therefore, we conclude that the initial fast decay of the anisotropy in small micelles cannot be due to residual bulk water.

An alternative explanation for the unusually fast decay of the anisotropy is the occurrence of *intermolecular* energy transfer, as happens in bulk water.^{28,29} However, in such a case, the anisotropy should decay monoexponentially on a sub-picosecond time scale to zero, which reflects a total depolarization of the sample. This is clearly in contradiction to the biphasic decay seen in micelles with $w_0 = 1$.

Another possible description is provided by the wobbling-in-a-cone model, which was used to explain the biphasic nature

of the anisotropy decay measured for HDO molecules solvated in the aqueous (H_2O) phase of reverse micelles.¹⁴ Using the wobble-in-a-cone description, the rotational motion of water was separated into two independent diffusion processes. A fast correlation time describes the early time decay of the anisotropy, arising from Brownian motion of the H_2O molecules on a cone characterized by its semiangle. An angular restriction at early times is imposed on the water molecules because they are strongly embedded in a hydrogen-bonded network. The long-time anisotropy decay is caused by orientational diffusion of the cone itself because of global structural rearrangements within the random H_2O network, and thereby leads to a full angular randomization of the water transition dipoles. Although being in qualitative agreement with our measurements, this model fails to explain the data in a quantitative manner. The calculations of Tan et al.¹⁴ demonstrated that the angular motions of the restricted rotor at early times are responsible for only 10% of the anisotropy decay in small micelles (consult Figure 3 and Table 2 in ref 14), which is well below the measured value of 50% in our experiments. In addition, the ~ 1 ps anisotropy decay time predicted by the wobbling-in-a-cone model¹⁴ is much longer than that obtained from our experiments (0.25 ps). Note that these considerations do not at all exclude the wobbling-in-a-cone effects from taking place in H_2O micelles; however, because of their small magnitude, they are screened by other, more pronounced processes.

The last option is that the biphasic decay of $R(\tau, \omega)$ originates from *intramolecular* flow of vibrational energy.⁴¹ The OH-stretching absorption line consists of two different sub-bands, which correspond to the quasi-orthogonal symmetric and asymmetric stretching modes. Although the absorption spectrum for small micelles shows some signatures of such substructure (Figure 2), the individual orthogonal resonances cannot be clearly identified because their spectral separation is comparable to the line widths. The fast anisotropy decay in this case is determined by the redistribution of population between the two modes on a time scale of ~ 0.2 ps, corresponding to their inversed spectral separation ($\sim 100 \text{ cm}^{-1}$). As the orientation of the normal modes is quasi-orthogonal, the anisotropy decays at a similar rate. This interpretation is also supported by a recent pump–probe study on isolated H_2O molecules dissolved in acetonitrile, where the anisotropy was shown to decay with time constants of 0.2 ± 0.1 ps and 2.5 ± 0.5 ps.⁴¹ The former time was ascribed to the intramolecular energy transfer between the symmetric and asymmetric modes, while the latter was related to the rotational diffusion of a water molecule. Since the anisotropy for micelles with $w_0 = 1$ corrected for thermalization component decays at the scale of tens of picoseconds, our data give evidence for much slower orientational dynamics of water confined to nanometer-sized droplets as compared to water in aqueous bulk samples or binary mixtures with acetonitrile.^{14,27,28,56} Most probably, this is due to a strongly hindered orientational mobility of water molecules induced by its interactions with the amphiphile ionic headgroups. A similar deceleration of the rotational dynamics has also been observed for water interacting with negatively charged ions in bulk solutions.⁶²

After validating in the previous paragraphs that no significant energy transfer occurs between interfacial molecules, we can investigate whether such an intermolecular relaxation channel exists between interfacial and core water molecules. The second and third columns in Figure 9 show typical anisotropy traces for $w_0 = 3$ and 8, where the core water fraction is around 20% and 50%, respectively. Again, the anisotropy decays faster when

the thermalization signal is not subtracted (red empty squares) than the $R(\tau)$ calculated according to eq 12 (blue dots). The thermalization-corrected anisotropy decay appears to be weakly dependent on the micelles size, and approaches time-independent values of 0.1–0.2 after 0.5 ps. This is an unambiguous indication that intermolecular energy transfer between the interfacial and core water must be *either very slow or does not exist at all*. If the interfacial and bulk water had exchanged energy on a 0.1–0.2 ps time scale, a total depolarization would have occurred on the very same time scale. This is clearly not the case and is in perfect agreement with the observed population kinetics (see section 5.1), where the two types of water were distinguished by their different vibrational lifetimes. Had the intermolecular energy transfer been efficient, the lifetimes of the interfacial and core water would have been comparable.

For sizes $w_0 = 3$ and 8, the anisotropy data are in reasonable agreement with predictions from the core/shell model. The anisotropy calculated for bulk fractions of 25% is shown in Figure 9h. The interfacial water was characterized by a lifetime of 0.85 ps and by a biexponential anisotropy decay with correlation times (relative amplitudes) of 0.26 ps (68%) and 10 ps (32%) (green solid line) taken from the measurements on micelles with $w_0 = 1$. For bulk-like water, we again used the data from ref 29. Figure 9i shows the simulated anisotropy for equal quantities of bulk and interfacial water (green solid line). At short times, the simulated $R(t)$ decays noticeably faster than the corresponding ($w_0 = 8$) experimental data, suggesting that the bulk depolarization time taken as 75 fs was underestimated.

Finally, the last column in Figure 9 shows the measurements for $w_0 = 35$. The anisotropy decay is essentially monoexponential, with a decay time without thermalization correction of 0.25 ± 0.1 ps and 0.12 ± 0.06 ps when the thermal signal is subtracted. In the latter case, the anisotropy decays not to zero but to an offset of ~ 0.1 –0.2 and then remains practically constant. Again, the decay can be qualitatively reproduced with the core/shell model using a bulk fraction of 85% (green solid curve in panel p)). However, the initial decay time seems to be faster than in the experiment, which is a direct consequence of the 75 fs anisotropy decay time taken for neat water. A substantially better correspondence is obtained when this value is increased to 0.25 ps (navy dashed curve), which is exactly the fast component of anisotropy for interfacial water (Figure 9,a–c). This observation strongly suggests that the depolarization of core water might have the same origin as for the shell water, namely, intramolecular energy flow. Note, that in previous studies on bulk water,^{28,29} the anisotropy was calculated directly from the pump–probe transients without any attempt to correct for the isotropic thermal contribution. As demonstrated above, this may lead to underestimated values of the anisotropy decay time.

It is instructive to compare the results of the anisotropy measurements on the H₂O-containing micelles with those on micelles filled with HDO diluted in H₂O^{14,16} or in D₂O.¹⁷ In the latter cases, the anisotropy decay becomes longer with decreased micelle size. In contrast, this trend is not so obvious for the H₂O-filled micelles (Figure 9), where anisotropy plots are quite similar for all sizes. For instance, the initial decay at the ~ 200 fs time scale that accounts for a 50% anisotropy loss is clearly seen for all sizes even before the thermalization signal is subtracted. The decay time of this component is between the expected values for inertial reorientations of ~ 50 fs⁵⁶ and the wobble-in-a-cone motion of 1–1.5 ps.^{14,16} In addition, the amplitudes of these components are far too small (typically, 10–20%) to account for the measured value of $\sim 50\%$.

Therefore, since neither time scale nor amplitude of the initial anisotropy decay in H₂O micelles match the inertial or wobble-in-a-cone motions, its origin must be different. In the smaller micelles, where the intermolecular coupling is excluded on the basis of the nonzero offset (Figure 9, two left columns), the intramolecular coupling of the two OH oscillators might be responsible for this phenomenon.⁴¹ In the larger micelles, the long-time offset is not that apparent because of the limited signal-to-noise ratio after the thermalization correction, and therefore the somewhat slower initial anisotropy decay as compared to bulk water^{28,29} might indicate the nanoconfinement effects. As far as the longer time scales are concerned, the anisotropy decay of tens of ps in small H₂O micelles is consistent with the HDO case.^{14,16,17} However, it is hard to say whether this tail becomes faster when the size increases, as is the case for the HDO–H₂O/D₂O micelles, because the experimental accuracy is limited by the extremely short population lifetime.

From the anisotropy data presented in this section, we can conclude that the intermolecular energy transfer previously reported for bulk water^{28,29} is strongly inhibited at least in the proximity of the membrane. A possible explanation for the inhibition of this process may be the presence of the sodium counterions that are most likely located near the ionic head-groups and therefore strongly perturb the hydrogen bond network of the interfacial water.^{26,50,51} The attractive forces between the water hydrogen atoms and the negative part of the surfactant heads might provide an explanation for the immobilization of the shell molecules. The rotational diffusion time for the interfacial water is definitely longer than 2 ps, most probably in the range of tens of picoseconds. The sub-picosecond anisotropy decay in the case of interfacial water is most likely due to an intramolecular energy conversion between modes with nonparallel transition dipole orientation.⁴¹ Although the intramolecular energy exchange might occur as well in the core water, the combination of the short vibrational lifetime and the strong thermalization signal preclude an unambiguous distinction between intra- and intermolecular processes. Our calculations (Figure 9p) clearly demonstrate that the anisotropy decays cannot be accurately reproduced using parameters from the available bulk water studies.^{28,29} This might be the result of true nanoconfinement effects in the entrapped water nanopool. Still, this conclusion is rather speculative, as long as no anisotropy studies on bulk H₂O in which the thermalization component has been properly¹⁶ dealt with, are available.

6. Summary and Conclusions

In this paper, the results of IR pump–probe experiments on neat H₂O confined in reverse micelles with $w_0 = 1$ –35 have been investigated. The most important feature of the neat water-filled micelles over diluted HDO mixtures is the resonant interaction among the densely packed hydroxyl groups. This interaction facilitates vibrational energy hopping from one excited OH oscillator to another,^{28,29} considerably accelerating processes like population relaxation,^{29,40,44,47,48} anisotropy decay,²⁸ and spectral diffusion.²⁹

To date, two different models have been proposed to explain the experimental results on neat H₂O inside reverse micelles. In the core/shell model,⁹ the water properties are affected only locally, near the boundary of the nanodroplet interface. In the homogeneous droplet model,¹² the water properties are identical throughout the nanodroplet as a fast intermolecular energy transfer wipes out any noticeable differences between the interfacial and core water.

In the discussion of the IR pump–probe measurements, we have shown that core and shell water have different population lifetimes, 0.27 and 0.85 ps, respectively. The 3-fold ratio of the relaxation times is larger than expected if the interfacial and core water follow the same relaxation pathway.¹² In addition, the build up of the thermalization signal is also consistent with a different relaxation mechanism for core and interfacial water. This scenario is further supported by the observation that the maximum transient temperature is lower in smaller micelles, suggesting that the excess vibrational energy of the interfacial water is not thermalized within the water droplet, as happens in the case of core water. Therefore, the vibrational energy of interfacial water relaxes through a different pathway than the core water, being most probably transferred directly to the AOT membrane.²⁰ The successful partitioning of the rotation-free transients for intermediate-sized micelles as well as FTIR spectra into bulk and interfacial components further support the core/shell model for neat water-filled micelles. This argument is substantiated because the weighting coefficients are in good agreement with the fractions of core and bulk water known from MD simulations⁵⁰ and NMR studies.⁵¹

Next to isotropic pump–probe kinetics, the transient anisotropy of water in reverse micelles has been investigated. The anisotropy data interpretation is complicated by the combined effect of a short lifetime and strong thermalization signal, which, if neglected, leads to overestimating the depolarization rate by more than 1 order of magnitude.

In small reverse micelles, the anisotropy decays to a nonzero offset with a characteristic time of 0.25 ± 0.1 ps, which is quite similar to the time scale of the ultrafast intramolecular energy transfer observed in isolated H₂O molecules.⁴¹ For large micelles and bulk water, this process is hardly distinguishable from the intermolecular energy transfer. When the thermalization signal is properly accounted for, the anisotropy of reverse micelles of different sizes persistently shows a slow component, with a decay time on the order of tens of picoseconds. This strongly suggests that the interfacial water molecules are less mobile than the bulk ones. Unfortunately, a more precise quantification of the long-time rotational diffusion is hindered by the short lifetime of the stretching mode.

On the basis of this study, we conclude that the water properties in the proximity of a membrane are different from the properties of bulk water. The membrane influences the water only locally, over a distance shorter than 0.4 nm,¹⁶ and thus it affects only one or two molecular layers. The anisotropy data for $w_0 = 1$ and $w_0 = 3$ prove that the shell molecules do not transfer the stretch energy to other water molecules for at least 2 ps, which is longer than twice the lifetime of interfacial water. NMR studies⁵¹ and MD simulations⁵⁰ suggest that the properties of water at the interface are mostly determined by strong interactions between water and the surface ions. These interactions disturb the hydrogen-bonding network, thereby preventing resonant vibrational energy transfer.^{28,29}

A clear difference should be made between interfacial and nanoconfinement effects. The first one refers to a localized effect, which is due to the interaction of H₂O molecules with the reverse micelles membrane as opposed to the water–water interactions that occur in the bulk. In contrast, the changes upon nanoconfinement reflect the reduction of cooperative effects due to the truncated hydrogen bond network. Therefore, true nanoconfinement effects should be visible only after removing the contribution from the interfacial water. In other words, if the nanoconfinement does influence the spectroscopic observ-

ables, the water in the micelle core should show different signatures than bulk water. Since the anisotropy in large micelles seems to decay slower than in bulk water, this might be indicative of true nanoconfinement effects on the water dynamics.

The conclusions presented above summarize all the information that could be obtained from IR pump–probe experiments on H₂O confined in AOT reverse micelles. A more powerful technique capable of revealing additional information is two-dimensional correlation spectroscopy.^{29,63,64} Such experiments, which will give direct access to ultrafast *dephasing* dynamics⁶⁵ and could provide a definite answer on the issue of the (im)mobility of the interfacial water, are underway.

Acknowledgment. We are grateful to Maaïke Milder for her contribution at the early stages of this project. The Deutsche Forschungsgemeinschaft (Grant No. Vo593/4-1) is acknowledged for financial support. This work is part of the research program of the “Stichting voor Fundamenteel Onderzoek der Materie (FOM)”, which is financially supported by the “Nederlandse Organisatie voor Wetenschappelijk Onderzoek (NWO)”.

Supporting Information Available: Details of the decomposition of FTIR reverse micelle spectra and simulations on micelle cooling. This material is available free of charge via the Internet at <http://pubs.acs.org>.

References and Notes

- Pal, S. K.; Peon, J.; Zewail, A. H. *Proc. Natl. Acad. Sci. U.S.A.* **2002**, *99*, 1763.
- Pal, S. K.; Zewail, A. H. *Chem. Rev.* **2004**, *104*, 2099.
- Pal, S. K.; Zhao, L.; Zewail, A. H. *Proc. Natl. Acad. Sci. U.S.A.* **2003**, *100*, 8113.
- Bürsing, H.; Kundu, S.; Vöhringer, P. *J. Phys. Chem. B* **2003**, *107*, 2404.
- Riter, R. E.; Undiks, E. P.; Levinger, N. E. *J. Am. Chem. Soc.* **1998**, *120*, 6062.
- Riter, R. E.; Willard, D. M.; Levinger, N. E. *J. Phys. Chem. B* **1998**, *102*, 2705.
- Levinger, N. E. *Science* **2002**, *298*, 1722.
- Douhal, A. *Chem. Rev.* **2004**, *104*, 1955.
- Cringus, D.; Lindner, J.; Milder, M. T. W.; Pshenichnikov, M. S.; Vöhringer, P.; Wiersma, D. A. *Chem. Phys. Lett.* **2005**, *408*, 162.
- Patzlaff, T.; Janich, M.; Seifert, G.; Graener, H. *Chem. Phys.* **2000**, *261*, 381.
- Seifert, G.; Patzlaff, T.; Graener, H. *Phys. Rev. Lett.* **2002**, *88*, 147402.
- Dokter, A. M.; Woutersen, S.; Bakker, H. J. *Phys. Rev. Lett.* **2005**, *94*, 178301.
- Tan, H. S.; Piletic, I. R.; Riter, R. E.; Levinger, N. E.; Fayer, M. D. *Phys. Rev. Lett.* **2005**, *94*, 057405.
- Tan, H. S.; Piletic, I. R.; Fayer, M. D. *J. Chem. Phys.* **2005**, *122*, 174501.
- Piletic, I. R.; Tan, H. S.; Fayer, M. D. *J. Phys. Chem. B* **2005**, *109*, 21273.
- Piletic, I. R.; Moilanen, D. E.; Spry, D. B.; Levinger, N. E.; Fayer, M. D. *J. Phys. Chem. A* **2006**, *110*, 4985.
- Dokter, A. M.; Woutersen, S.; Bakker, H. J. *Proc. Natl. Acad. Sci. U.S.A.* **2006**, *103*, 15355.
- Rička, J.; Borkovec, M.; Hofmeier, U. *J. Chem. Phys.* **1991**, *94*, 8503.
- Pileni, M. P. *Structure and Reactivity in Reverse Micelles*; Elsevier: Amsterdam, 1989.
- Deak, J. C.; Pang, Y.; Sechler, T. D.; Wang, Z.; Dlott, D. D. *Science* **2004**, *306*, 473.
- De, T. K.; Maitra, A. *Adv. Colloid Interface Sci.* **1995**, *59*, 95.
- Onori, G.; Santucci, A. *J. Phys. Chem.* **1993**, *97*, 5430.
- Fiochetto, D.; Freda, M.; Mannaioli, S.; Onori, G.; Santucci, A. *J. Phys. Chem. B* **1999**, *103*, 2631.
- Fiochetto, D.; Freda, M.; Onori, G.; Santucci, A. *J. Phys. Chem. B* **1999**, *103*, 8216.
- Freda, M.; Onori, G.; Paciaroni, A.; Santucci, A. *J. Mol. Liq.* **2002**, *101*, 55.
- Faeder, J.; Ladanyi, B. M. *J. Phys. Chem. B* **2001**, *105*, 11148.
- Cringus, D.; Yeremenko, S.; Pshenichnikov, M. S.; Wiersma, D. A. *J. Phys. Chem. B* **2004**, *108*, 10376.

- (28) Woutersen, S.; Bakker, H. J. *Nature* **1999**, 402, 507.
- (29) Cowan, M. L.; Bruner, B. D.; Huse, N.; Dwyer, J. R.; Chugh, B.; Nibbering, E. T. J.; Elsaesser, T.; Miller, R. J. D. *Nature* **2005**, 434, 199.
- (30) Rey, R.; Møller, K. B.; Hynes, J. T. *J. Phys. Chem. A* **2002**, 106, 11993.
- (31) Lawrence, C. P.; Skinner, J. L. *J. Chem. Phys.* **2002**, 117, 8847.
- (32) Lawrence, C. P.; Skinner, J. L. *Chem. Phys. Lett.* **2003**, 369, 472.
- (33) Schwarzer, D.; Lindner, J.; Vöhringer, P. *J. Chem. Phys.* **2005**, 123, 161105.
- (34) Schwarzer, D.; Lindner, J.; Vöhringer, P. *J. Phys. Chem. A* **2006**, 110, 2858.
- (35) The observation made in ref 9 that the width of the linear absorption spectrum is maximal for $w_0 = 10$ sizes was erroneous, as immediately follows from inspection of Figure 1 of the same reference.
- (36) Yeremenko, S.; Baltuska, A.; de Haan, F.; Pshenichnikov, M. S.; Wiersma, D. A. *Opt. Lett.* **2002**, 27, 1171.
- (37) Gordon, R. G. *J. Chem. Phys.* **1966**, 45, 1643.
- (38) Tan, H. S.; Piletic, I. R.; Fayer, M. D. *J. Opt. Soc. Am. B* **2005**, 22, 2009.
- (39) Hamm, P.; William, M. L.; DeGrado, F.; Hochstrasser, R. M. *Proc. Natl. Acad. Sci. U.S.A.* **1999**, 96, 2036.
- (40) Lindner, J.; Vöhringer, P.; Pshenichnikov, M. S.; Cringus, D.; Wiersma, D. A.; Mostovoy, M. *Chem. Phys. Lett.* **2006**, 421, 329.
- (41) Cringus, D.; Jansen, T. I. C.; Pshenichnikov, M. S.; Wiersma, D. A. *J. Chem. Phys.* **2007**, 127, 084507.
- (42) Hare, D. E.; Sorensen, C. M. *J. Chem. Phys.* **1990**, 93, 6954.
- (43) Senior, W. A.; Verrall, R. E. *J. Phys. Chem.* **1969**, 73, 4242.
- (44) Lock, A. J.; Woutersen, S.; Bakker, H. J. *J. Phys. Chem. A* **2001**, 105, 1238.
- (45) Asbury, J. B.; Steinel, T.; Stromberg, C.; Gaffney, K. J.; Piletic, I. R.; Fayer, M. D. *J. Chem. Phys.* **2003**, 119, 12981.
- (46) Gaffney, K. J.; Davis, P. H.; Piletic, I. R.; Levinger, N. E.; Fayer, M. D. *J. Phys. Chem. A* **2002**, 106, 12012.
- (47) Lock, A. J.; Bakker, H. J. *J. Chem. Phys.* **2002**, 117, 1708.
- (48) Ashihara, S.; Huse, N.; Espagne, A.; Nibbering, E. T. J.; Elsaesser, T. **2007**, 111, 743.
- (49) Miller, R. E. *Science* **1988**, 240, 447.
- (50) Faeder, J.; Ladanyi, B. M. *J. Phys. Chem. B* **2000**, 104, 1033.
- (51) Maitra, A. J. *Phys. Chem.* **1984**, 88, 5122.
- (52) Bürsing, H.; Vöhringer, P. *Phys. Chem. Chem. Phys.* **2000**, 2, 73.
- (53) Bürsing, H.; Lindner, J.; Hess, S.; Vöhringer, P. *Appl. Phys. B* **2000**, 71, 411.
- (54) Winkler, K.; Lindner, J.; Bürsing, H.; Vöhringer, P. *J. Chem. Phys.* **2000**, 113, 4674.
- (55) Laage, D.; Hynes, J. T. *Science* **2006**, 311.
- (56) Loparo, J. J.; Fecko, C. J.; Eaves, J. D.; Roberts, S. T.; Tokmakoff, A. *Phys. Rev. B* **2004**, 70, 180201.
- (57) Rezus, Y. L. A.; Bakker, H. J. *J. Chem. Phys.* **2005**, 123, 114502.
- (58) Steinel, T.; Asbury, J. B.; Zheng, J.; Fayer, M. D. *J. Phys. Chem. A* **2004**, 108, 10957.
- (59) Bürsing, S. H. H.; Vöhringer, P. *J. Chem. Phys.* **1999**, 111, 5461.
- (60) Graener, H.; Seifert, G. *J. Chem. Phys.* **1992**, 98, 36.
- (61) Lindner, J.; Vöhringer, P.; Pshenichnikov, M. S.; Cringus, D.; Wiersma, D. A. Anharmonic bend–stretch coupling in water. In *Ultrafast Phenomena XV*; Corkum, P., Jonas, D., Miller, D., Weiner, A. M., Eds.; Springer: Pacific Grove, CA, 2006.
- (62) Kropman, M. F.; Bakker, H. J. *Science* **2001**, 291, 2118.
- (63) Khalil, M.; Demirdoven, N.; Tokmakoff, A. *J. Phys. Chem. A* **2003**, 107, 5258.
- (64) Kwac, K.; Lee, C.; Jung, Y.; Han, J.; Kwak, K.; Zheng, J. R.; Fayer, M. D.; Cho, M. *J. Chem. Phys.* **2006**, 125, 244508.
- (65) Lazonder, K.; Pshenichnikov, M. S.; Wiersma, D. A. *Opt. Lett.* **2006**, 31, 3354.